Estuarine, Coastal and Shelf Science 329 (2026) 109650

Contents lists available at ScienceDirect

Estuarine, Coastal and Shelf Science

journal homepage: www.elsevier.com/locate/ecss

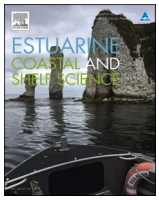

Alternate rotating layered circulation in response to extrinsic and intrinsic forcing in the Japan sea

Junlu Li [a,b], Jianping Gan [b,*]

[a] School of Marine Sciences, Sun Yat-Sen University, Southern Marine Science and Engineering Guangdong Laboratory (Zhuhai), Zhuhai, China
[b] Center for Ocean Research in Hong Kong and Macau and Department of Ocean Science, The Hong Kong University of Science and Technology, Hong Kong, China

ARTICLE INFO

Keywords:
Japan sea
Rotating layered circulation
Vorticity dynamics
Numerical model

ABSTRACT

The three-dimensional circulation in the Japan Sea (JS) plays an important role in its water mass and biogeochemical substances exchange with neighboring oceans. However, characterizing the spatiotemporal circulation pattern in the JS, and diagnosing its complex forcing mechanism between intrinsic flow-topography interaction and extrinsic flux through the straits connected with adjacent seas remain challenge. Combined observations with numerical modeling and a novel Stokes-based layer-integrated vorticity equation (LIVE) dynamics, we discovered a three-layer circulation with alternating cyclonic, anti-cyclonic, and cyclonic circulation in the upper (0–150 m), middle (150–250 m), and bottom (>250 m) layers in the JS, respectively. The strong cyclonic and weak anti-cyclonic circulations in the upper and middle layers show similar seasonal phase: the domain-integrated vorticity anomaly is positive during winter and negative from summer to early autumn. In contrast, cyclonic circulation in the bottom layer remains relatively stable throughout the year. We diagnosed that besides vorticity input from wind stress curl in the upper layer, the lateral planetary vorticity fluxes from inflow/outflow through the straits surrounding the JS lead to vortex stretching in all layers and extrinsically control the structure of the layered circulation. The joint effects of baroclinicity and relief (JEBAR) arising from flow–topography interaction is an intrinsic dynamic response to the extrinsic forcing and dynamically shapes the layered circulation. Based on Stokes circulation theorem, this study characterizes the layered circulation pattern, and based on LIVE dynamics, effectively identifies intrinsic and extrinsic forcing mechanisms for the layered circulation in the JS and other marginal seas.

1. Introduction

The Japan Sea (JS), also known as the East Sea, is a semi-closed marginal sea located in the western North Pacific with a deep basin that exceeds 4000 m in depth (Fig. 1a). The Yamato Rise (YR) at the center of the JS divides the basin into three distinct regions: the Ulleung Basin (UB) in the southwest, the Yamato Basin (YB) in the southeast, and the Japan Basin (JB) in the north.

The circulation in the JS is primarily influenced by atmospheric forcing and the lateral influx and outflux of water through four major straits: the Tsushima, Tsugaru, Soya, and Tartary Straits. The four straits connect the JS to adjacent seas (Fig. 1a). The Tsushima Strait (TSM), in the southwest, links the JS to the East China Sea. Salty warm water originating from the Kuroshio Current (Lie and Cho, 1994) enters the JS through the TSM, bifurcating into three currents: the Tsushima Current, the East Korea Warm Current, and the East Sea Current (Kawabe, 1982; Kim and Yoon, 2010).

The Tsushima Current flows northeastward along the west coast of Japan and exits the JS through Tsugaru Strait (TGR) and Soya Strait (SOY). The East Korea Warm Current flows east of Korea and splits into two branches. The offshore branch, the East Sea Current, turns eastward and passes across the center of the JS to join the Tsushima Current near TGR, and the primary branch of the East Korea Warm Current, attached to the east coast of Korea, flows northward and converges with the southward North Korea Cold Current (Kawabe, 1982; Chang et al., 2004).

At the western boundary of the Japan Basin, the Liman Cold Current flows southward along the east coast of Russia, forming the origin of the North Korea Cold Current. Tartary Strait (TTR) connects the JS to the Sea of Okhotsk but has limited water mass exchange (Yanagi, 2002), effectively closing the basin's circulation at the north of the JS. Thus, the large cyclonic circulation in the north of JS and the anti-cyclonic

* Corresponding author.
E-mail address: magan@ust.hk (J. Gan).

https://doi.org/10.1016/j.ecss.2025.109650
Received 26 May 2025; Received in revised form 13 November 2025; Accepted 2 December 2025
Available online 2 December 2025

circulation in the Ulleung Basin and the Yamato Basin (Kim and Kim, 1999) form the upper layer circulation in the JS. The basins and major currents in the upper layer of the JS are shown in Fig. 1a and c with their respective abbreviations.

Previous studies primarily focused on the JS upper layer circulation dynamics and how the upper layer circulation forms. Those studies found that, for the annual mean state, atmospheric forcing (Kim and Yoon, 2010), lateral fluxes through the surrounding straits, and thermal structure (Chang et al., 2002; Kim and Yoon, 2010; Yi, 1982) all control the upper layer's flow pattern. In addition, the intrusion of water through the (TSM) and its three branches are significant in consolidating the cyclonic gyre in most areas of the JS's upper layer (Chang et al., 2002).

Historic calculations of the volume transport across the TSM have been varied. These earlier estimates were based on dynamical calculation with a chosen reference depth, a velocity derived from sea level differences, and moored acoustic Doppler current profiler (ADCP) and shipboard ADCP data. The annual mean TSM transport calculations range from 0.5 to 4.2 Sv, with significant seasonal variation (Byun and Seung, 1984; Isobe et al., 1994; Miita and Ogawa, 1984; Takikawa et al., 2005; Tawara et al., 1984; Teague et al., 2002; Yi, 1966). The Tsushima Current and the East Sea Current, two of the branches of the TSM intrusion, export water from the JS through the TGR with an annual mean transport of ~1.5 Sv (Ito et al., 2003; Nishida et al., 2003; Toba et al., 1982), and through SOY with a variable transport ranging from 0.5 to 1.5 Sv (Fukamachi et al., 2010; Matsuyama et al., 2006). The volume transport influx through TSM and outflux through SOY vary significantly seasonally and in-phase with maxima during early autumn and minima during winter. In contrast, the TGR outflux transport is weakly seasonal (Han et al., 2016). We have found that, despite the transport of each strait having been widely investigated with observations and model simulations, the dynamic connection between the lateral fluxes and the circulation within the JS is still unclear.

In addition, very little is known about the subsurface circulation in the JS, especially the spatiotemporal characteristics of the circulation below pycnocline, and the corresponding mechanisms at different layers. Previous research into the middle and bottom layers of the JS circulation has primarily focused on water mass properties and water formation rather than the circulation patterns themselves (Gamo and Horibe, 1983; Kim and Kim, 1999; Senjyu, 1999; Yoon and Kawamura, 2002). Yoon and Kawamura (2002) claimed that the salinity minimum and dissolved oxygen maximum in the middle layer originate from the Liman Cold Current, which subducts below the warm water in the southwestern JS. Gamo and Horibe (1983) discussed the unique potential temperature and dissolved oxygen of the deep and bottom water below 1000 m and suggested that the deep and bottom water form in the southern and northwestern JS, respectively. Since 1996, observations targeting the subsurface and deep layers of the JS have been made, particularly in the Ulleung Basin (Chang et al., 2002; Teague et al., 2005) and the Japan Basin (Takematsu et al., 1999). These observations have revealed that there is an energetic deep circulation in the JS. However, due to the limited resolution and coverage in space and time, these observations cannot provide a holistic view of the deep layer circulation for the entire JS.

Nevertheless, efforts have been made to holistically unveil the circulation in the JS using a combination of observations and model simulations. Yet, because of the challenges of deploying deep-sea equipment and the complexity of the circulation's dynamics, it is difficult to achieve

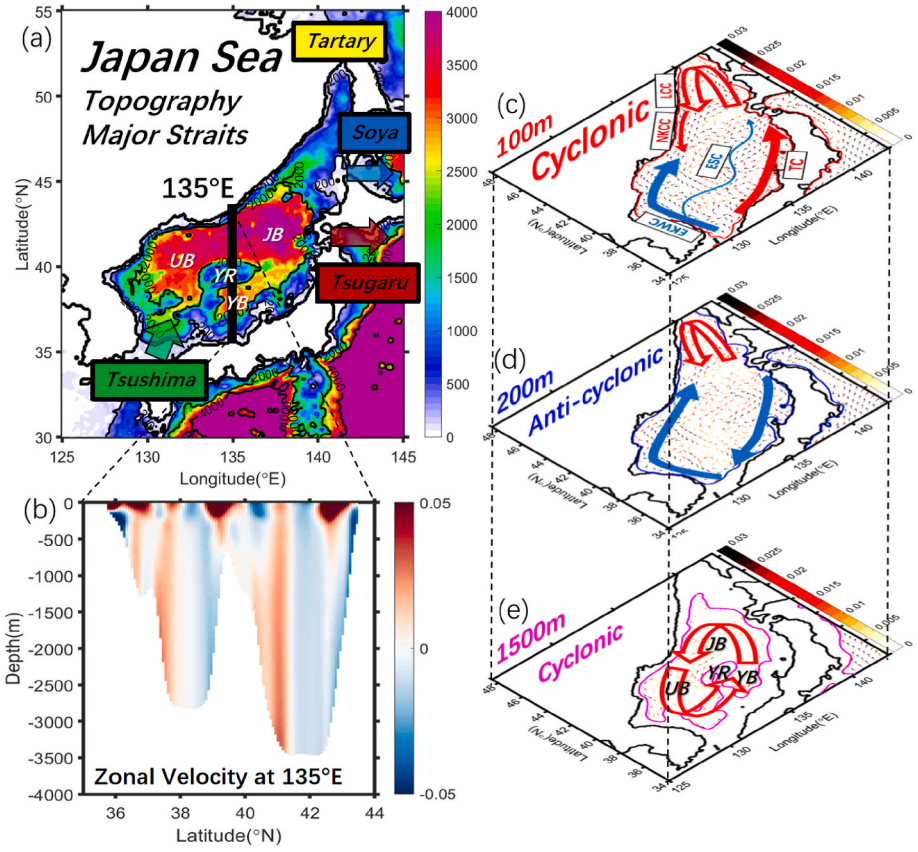

Fig. 1. (a) Topography and main straits of the Japan Sea. YR denotes the Yamato Rise. UB, YB, and JB denote the Ulleung Basin, Yamato Basin, and Japan Basin, respectively. (b) Annual mean zonal velocity at the 135°E section. A positive value denotes eastward velocity. Annual mean vorticity and isobaths of (c) 100 m, (d) 200 m, and (e) 1500 m depth. In (c), (d) and (e), the vectors show the velocity direction, and the color indicates the velocity magnitude. The arrows denote the direction of the main flows, including the Tsushima Current (TC), East Korea Warm Current (EKWC), East Sea Current (ESC), North Korea Cold Current (NKCC) and Liman Cold Current (LCC). (For interpretation of the references to color in this figure legend, the reader is referred to the Web version of this article.)

a comprehensive dynamic understanding of the three-dimensional, time- and depth-dependent JS circulation. In this study, we not only systematically show the characteristics of layered circulation in the JS, but also use a novel layered integrated vorticity dynamics to provide insight into coupled extrinsic and intrinsic controls on the layered circulation. Knowing why the three-layered circulation occurs and forms can help us understand the marginal JS water mass distribution, and how the seasonal exchange with the neighboring seas occurs. For the prospect of this work, our new knowledge of the JS circulation dynamics will provide a better understanding of how biogeochemical properties will be seasonally distributed within the JS basins.

2. Data and method

2.1. Numerical ocean model

Using the China Sea Multiple-scale Ocean Modeling System (CMOMS) (Gan et al., 2016a, 2016b), we conducted a process-oriented study that revealed details of the JS circulation dynamics. CMOMS is based on the Regional Oceanic Modeling System (ROMS) (Shchepetkin and McWilliams, 2005) and has sufficient resolution and coverage for the JS. The vertical mixing parameterization of the model is based on a local closure scheme using the level-2.5 turbulent kinetic energy equations (Mellor and Yamada, 1982). The model covers the entire China Sea, the JS, and the western part of the tropical North Pacific. We generated the coastline and bathymetry by merging ETOPO5 data from the National Geophysical Data Center with digitized water depths extracted from navigation maps published by the China Maritime Safety Administration. The model has a horizontal resolution of ~8 km in the JS, which can resolve the meso-scale variability. Vertically, we used 30-layer stretched terrain-following coordinates with denser resolution at the pycnocline and bottom boundary layers.

To realistically simulate the JS circulation, we forced the model with wind stress derived from daily sea surface winds released by the National Oceanic and Atmospheric Administration (NOAA). In addition, we forced the model with the heat/salt flux from daily reanalysis meteorological data provided by the National Centers for Environmental Prediction (NCEP) based on a bulk formulation (Fairall et al., 2003). For the open boundary conditions, we applied the integrated active open boundary conditions (Gan and Allen, 2005) and Tidal-Subtidal open boundary conditions (Liu and Gan, 2016) to resolve the tidal and subtidal forcing at the eastern and southern boundaries of the model domain. We also used the Ocean General Circulation Model for the Earth Simulator (OFES) (Sasaki et al., 2008) to provide the three-dimensional velocity, temperature, and salinity, and the sea level elevation for the lateral boundary conditions.

We applied the climatological atmospheric forcing and lateral fluxes from NOAA, NCEP, and OFES for a period of 50 years to force the model to reach a steady state. The variables averaged during the boreal winter (November, January, and February) of the final five years of the steady state run (years 46–50) produced the initial conditions for the realistic simulation. Subsequently, we spun up the model from 1988 and forced it with realistic forcings and lateral fluxes adopted from an OFES hindcast. For this study, we used monthly climatological results averaged over 20 years from 1993 to 2012 to demonstrate the annual cycle of the JS circulation and perform our physical and dynamic analyses.

2.2. Observations

To reveal details of the JS circulation and to validate our model results, we used two sets of observations. The first data set was the geostrophic velocity field calculated from temperature and salinity provided by the U.S Navy Generalized Digital Environment Model (GDEM, version 3.0, Carnes, 2009), based on the thermal wind relation. The gridded GDEM data is generated by 4.5 million observed temperature and salinity profiles from 1920 onward, with a horizontal resolution of 0.25°and a vertical resolution ranging from 2 m at the surface to 200 m at the bottom. To derive the geostrophic velocity, we used 500 m as the level of no motion. Our 500 m level of no motion is reasonably based on the layered circulation previously observed in the JS and the domain-averaged velocity magnitude in the JS adopted from models and other observations. The 500 m is less than 5 % of the maximum magnitude of the whole water column (Shin et al., 1996; Chang et al., 2002). The second data set was the monthly mean velocity field adopted from the Ocean Reanalysis System 5 (ORAS5) released by the European Centre for Medium-Range Weather Forecasts (ECMWF). The ORAS5 combines model data with complete and consistent observations based on the laws of physics and provides historic and current ocean variables starting from 1958. The horizontal resolution of ORAS5 is 0.25°, and the vertical resolution ranges from meters near the surface to hundreds of meters at the bottom.

3. Results

3.1. Three-layer basin circulation

Following Gan et al. (2016a), we linked the circulation to the domain-integrated vorticity of each layer. Stokes' theorem states:

$$\Gamma = \oint_l \boldsymbol{V}_s dl = \iint_A \zeta dA \tag{1}$$

where Γ is the intensity of the circulation, $\boldsymbol{V}_s$ is the along-boundary velocity of a specific domain, and ζ is the vorticity normal to the specific domain with an area of A.

The annual mean velocity vectors at 100 m, 200 m, and 1500 m displayed in Fig. 1b represent the typical circulation patterns in the upper, middle, and bottom layers of the JS, respectively. The red (blue) arrows represent the currents and circulations that contribute to the cyclonic (anti-cyclonic) vorticity. In the upper layer, cyclonic vorticity dominates, although the Korea Warm Current provides a small area of anti-cyclonic vorticity in the Ulleung Basin in the southwest JS. The northern JS is occupied by a stable cyclonic gyre, and the southeastern Yamato Basin is occupied by the Tsushima Current. In the middle layer, the Tsushima Current is replaced by a southwestward flow, resulting in an anti-cyclonic gyre dominating the southern JS. Compared to the upper layer, once the circulation combines with the weakened cyclonic gyre in the northern JS, the circulation in the middle layer becomes anti-cyclonic. In the bottom layer, the basin is separated by the Yamato Rise, and the bottom current flows cyclonically and is attached to the slope, forming a persistent cyclonic circulation. The zonal velocity profile along 135°E demonstrates the vertical structure of the cross-basin transect (Fig. 1b). It is notable that strong currents only exist in the upper ~250 m or are attached to the slopes. In the middle of the basins, the current speed is small.

Stoke's Theorem helps us clearly illustrate the vertical structure in the entire JS at each depth using results from the model, GDEM, and ORAS5 data sets (Fig. 2a and b), respectively. Qualitatively, our findings show that there is strong positive vorticity in the upper layer, weak negative vorticity in the middle layer, and positive vorticity in the bottom layer, although the layers are not at the same depths. Our model separated the three layers at 150 m and 250 m. For the observations, the separation depths were deeper, which might have been because of the limited number of subsurface observations. To further confirm the three-layer structure, we compared our results with the widely used global model of OFES and the Hybrid Coordinate Ocean Model (HYCOM), both of which exhibited the same three-layer structure (not shown). Therefore, we were assured our results were valid, and we could reliably use the CMOMS results to analyze the characteristics, variabilities, and dynamics of the circulation.

According to the vertical profile of the domain-integrated vorticity shown in Fig. 2a, we defined the upper, middle, and bottom layers as

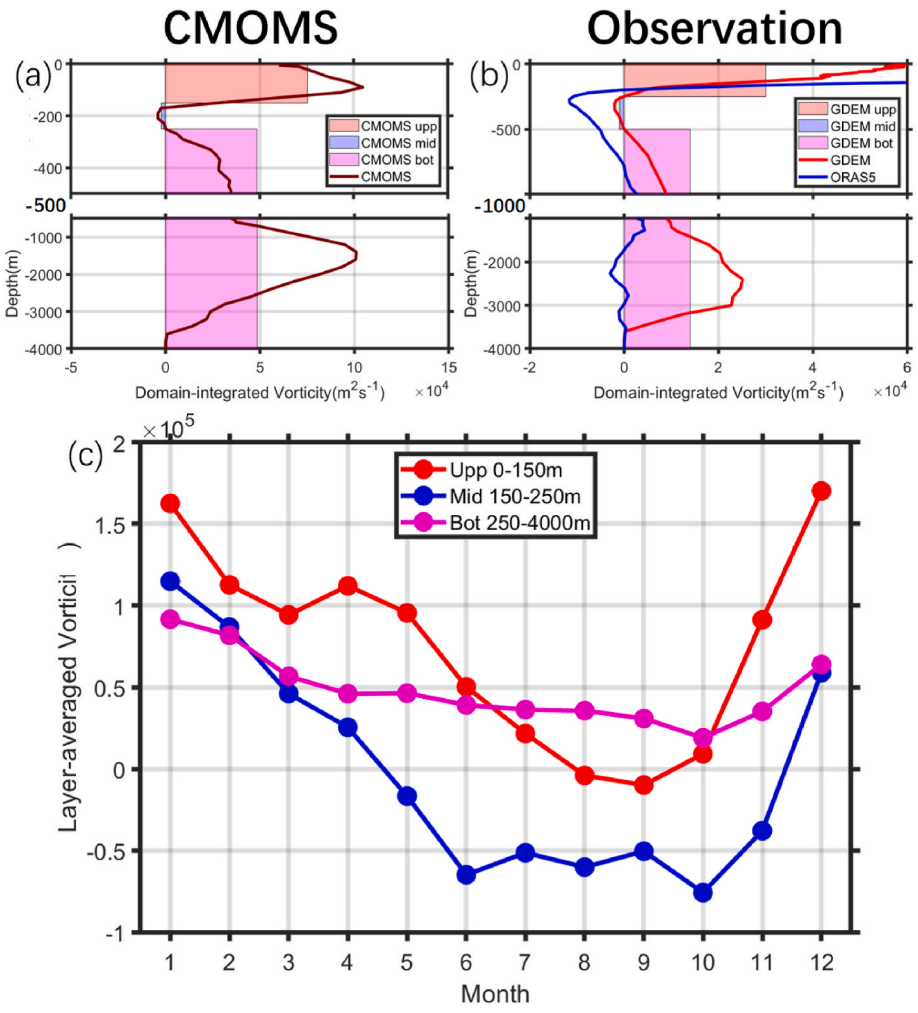

Fig. 2. Vertical profile of the annual mean domain-integrated vorticity obtained from (a) CMOMS and (b) observations: GDEM and ORAS5. (c) Monthly depth-averaged domain-integrated layer vorticity for a one-year cycle obtained from CMOMS results.

0–150 m, 150–250 m, and 250–4000 m, respectively. In Fig. 2c, we see that the three layers have unique seasonal variations. In the upper layer, the circulation is strongly positive during the winter, with the magnitude of domain-integrated vorticity reaching maximum of 1.7×10^5 m^2/s in December, and weakly negative in early autumn with minimum of -1×10^4 m^2/s in September. The middle layer circulation has a seasonal phase similar to the upper layer circulation: positive during winter and negative from summer to autumn, with the magnitude of domain-integrated vorticity ranging from -7.5×10^4 m^2/s in October to 1.1×10^5 m^2/s in January. The amplitudes of $\sim 1.8 \times 10^5$ m^2/s in the upper- and middle-layer circulation indicate their significant seasonal variation. In contrast, the bottom layer circulation remains stably positive throughout the year, with the magnitude of domain-integrated vorticity ranging from 2×10^4 m^2/s in October to 9×10^4 m^2/s in January. The in-phase seasonality in the circulation of the upper and middle layers correlates with the wind stress curl forcing. The correlation suggests that the atmospheric flux affects the water column at depths shallower than 250 m, including the Ekman depth of ~100 m in this region, as well as the penetration depth to the 250 m through baroclinic pathway.

3.2. Exchange with adjacent ocean

The circulation pattern in the upper layer of the JS is influenced by wind stress curl and by the inflowing and outflowing volume transports, or by the corresponding lateral planetary vorticity, through the three major straits of the TSM, TGR, and SOY. The annual mean cross-section velocity profiles from the four straits are shown in Fig. 3a, b, c, and d. The volume transport through the TTR is small and equivalent to a closed boundary, as has been previously reported; for example, by Yanagi (2002) (Fig. 3a). A northward velocity dominates the TSM, and an eastward velocity dominates the SOY and TGR. The TSM provides the saline and warm water influx to the JS throughout the year, and the SOY and TGR are exits for the JS water. The annual mean volume transports of the TSM, TGR, and SOY are ~2.5 Sv, ~1.5 Sv, and ~0.7 Sv, respectively. The annual mean and seasonal variations of these straits' transports are basically consistent with previous observations and other model results (Han et al., 2016) (Fig. 3e). The observations (OBS) include: vessel-mounted ADCP data in TSM covering most time from 1997 to 2012, bottom-mounted ADCP data and sea level regressed transport in TGR from 1993 to 2012 and bottom-mounted ADCP data and high-frequency radar data in SOY from 2004 to 2008. The multiple-model ensembles (MOD) include four different ocean data assimilation models: the Data Assimilation Research of the East Asian Marine System, the Meteorological Research Institute Multivariate Ocean Variational Estimation System/Meteorological Research Institute Community Ocean Model, the Japan Coastal Ocean Predictability Experiment, and HYCOM. There are many reasons that may cause the deviation between the model and observation, such as lack of sufficient resolution and sub-mesoscale processes in the model as well as non-synchronized observational measurements. The TSM and SOY transports are strongly seasonal, reaching maxima in late autumn and minima in winter, whereas the TGR transport is weakly seasonal. The

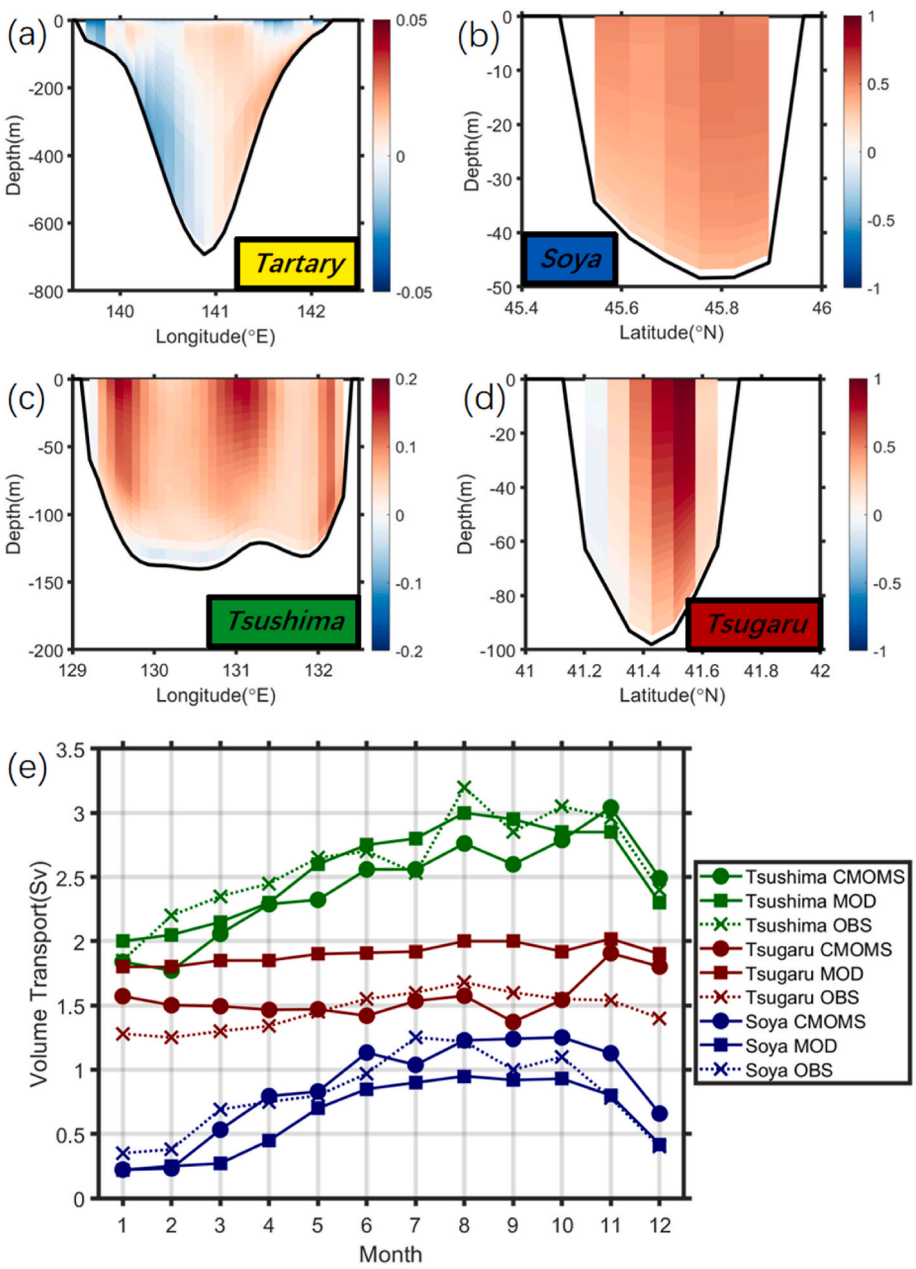

Fig. 3. Annual mean cross-section velocity profiles from the (a) Tartary, (b) Soya, (c) Tsushima, and (d) Tsugaru Straits. Positive values denote northward (eastward) velocity for the Tartary/Tsushima (Soya/Tsugaru) Straits. (e) Climatological annual cycle of volume transports at the Tsushima, Tsugaru and Soya Straits obtained from CMOMS results, and other models (MOD) and observations (OBS) from Han et al. (2016).

seasonality in the TSM and SOY transports is consistent with the domain-integrated vorticity in the upper and middle layers, suggesting a physical connection between the current intensity and the circulation strength.

4. Discussion

4.1. Layered integrated vorticity equation (LIVE)

By applying Equation (1) to the depth-integrated momentum and vorticity equation for each layer, we isolated the different physical processes and dynamics that control the entire JS circulation. This domain- and layer-integrated vorticity equation (LIVE) was presented by Gan et al. (2016a) and is written as:

$$\Omega_{acc} = \Omega_{cor} + \Omega_{hadv} + \Omega_{hvisc} + \Omega_{pgf} + \Omega_{vadv} + \Omega_{vvisc} \quad (2)$$

The acceleration term, Ω_{acc}, represents the domain-integrated vorticity change with time. The terms on the right-hand side of Equation (2) represent the effects of the divergence Ω_{cor}, the horizontal advection Ω_{hadv}, the horizontal viscosity Ω_{hvisc}, the bottom pressure torque Ω_{pgf}, the vertical advection Ω_{vadv}, and the vertical viscosity Ω_{vvisc}, respectively. The bottom pressure torque, Ω_{pgf}, indicates the curl of the horizontal component of the force normal to the bottom, which is exerted by the physical bottom on the fluid (Mertz and Wright, 1992). Ω_{vvisc} gives the net effect of the horizontal stress curl at the surface (Ω_{sstr}) and bottom (Ω_{bstr}). We applied Equation (2) to each layer following Gan et al. (2016a).

To further separate the extrinsic forcing and intrinsic dynamics in the layered circulation, we adopted a divergence theorem to transform Ω_{cor}:

$$\Omega_{cor} = \oint_l f \mathbf{V_n} dl, \quad (3)$$

where l is the lateral boundaries of the domain. f is the planetary vorticity, and $\boldsymbol{V_n}$ is the inward velocity normal to the boundaries. Because of the mathematical operation in Equation (3), Ω_{cor} physically represents the net planetary vorticity flux across the straits that surround the JS. In other words, the net planetary vorticity flux across all the straits represents extrinsic forcing dynamics.

This dynamic approach has been successfully applied to the South China Sea (Gan et al., 2016a) and the undercurrent system in the tropical western North Pacific (Li and Gan, 2020) and has proven effective in quantifying the contributions of isolated physical mechanisms from extrinsic and intrinsic forcing to the layered circulation in JS. In this study, we applied this method to explore the physical processes and underlying dynamics that regulate the circulation in each layer of a new important region: the JS.

4.2. Coupled extrinsic and intrinsic forcing mechanism

To examine the forcing dynamics and to quantify the contributions of different physical processes, we calculated the terms in Equation (2) for the three layers during winter and summer (Fig. 4).

In the upper layer, the circulation is strongly cyclonic in winter and weakly anti-cyclonic in summer. The positive Ω_{sstr} induced by the wind stress curl and the Ω_{pgf} provided by the joint effects of baroclinicity and relief (JEBAR) are the two main contributors to the strong cyclonic circulation. The positive Ω_{sstr} is mainly offset by negative Ω_{cor} due to the residual planetary vorticity and Ω_{hadv} as an intrinsic nonlinear process (Fig. 4c). Compared to the circulation in winter, the weak anti-cyclonic circulation in summer is due to the stronger negative Ω_{cor} and weaker positive Ω_{sstr} (Fig. 4d). The negative Ω_{cor} throughout the year is caused by the TSM transport which brings water with a small planetary vorticity into the JS, while the water with large planetary vorticity exits the JS through the SOY and TGR (Fig. 4a and b), leading to a negative net planetary vorticity. Ω_{bstr} is an important compensation term, which decelerates the circulation throughout the year. In summer and winter, Ω_{bstr} and Ω_{pgf} have opposite signs, suggesting the interaction and correlation between the bottom stress curl and JEBAR related to the slope topography. The seasonal variation of the upper layer basin-scale vorticity can be attributed to the change of strait fluxes and wind forcing. Specifically, an enhanced strait fluxes from winter to summer (Fig. 3e) result in additional negative planetary vorticity in the basin (Fig. 4a and b). Meanwhile, the wind stress curl is also weakened from strong positive to weak positive during this time, as indicated by Ω_{sstr} (Fig. 4c and d). These two extrinsic forcings drive the domain-integrated vorticity from strong positive to weak negative value (Fig. 2c), accompanying with corresponding intrinsic processes discussed above.

In the middle layer, the circulation changes dramatically from cyclonic in winter to anti-cyclonic in summer. The depth of the middle layer (150–250 m) is below the deepest point of the TSM (~140 m), TGR (~100 m), and SOY (~50 m) as shown in Fig. 3. Therefore, Ω_{cor} is only

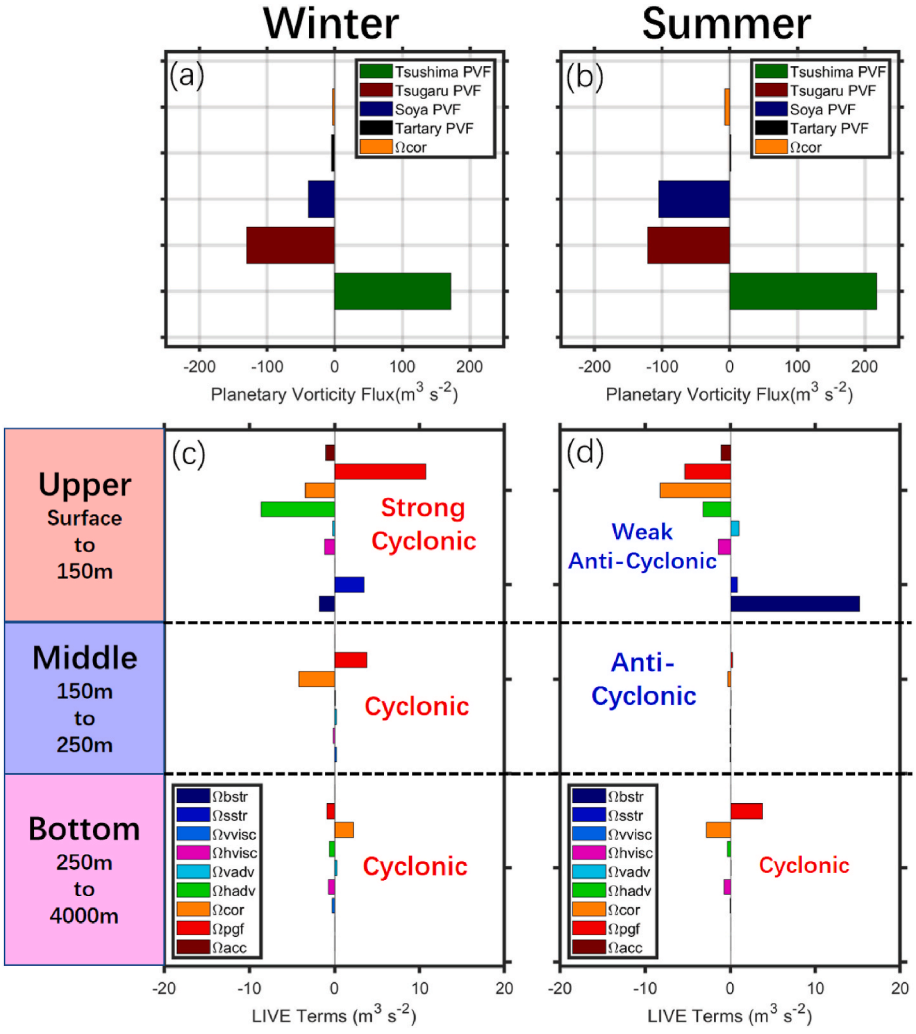

Fig. 4. Planetary vorticity fluxes through the four straits of the JS in (a) winter and (b) summer. Dynamic terms calculated from the vorticity balance-based equation, LIVE (Gan et al., 2016b) in the upper, middle and bottom layers of the JS in (c) winter and (d) summer.

controlled by the planetary vorticity flux through the TTR. At this depth, Ω_{pgf} and Ω_{cor} basically compensate for each other, while the other terms are negligible. Ω_{pgf} dominates in winter and Ω_{cor} dominates in summer, resulting in the varying circulation.

In the bottom layer, the circulation remains cyclonic throughout the year, and is weaker in summer than in winter. Ω_{cor} indicating that the planetary vorticity influx through the TTR dominates the positive vorticity in winter. In contrast, Ω_{pgf} induced by the bottom pressure torque offsets Ω_{cor}, leaving a residual portion contributing to the positive vorticity in summer.

5. Conclusion

By combining data from multiple sources and 3D numerical modeling, we have revealed the structure and spatiotemporal variation of the three-layer circulation in the JS. The layered circulation is characterized by cyclonic circulation, anti-cyclonic circulation and cyclonic circulation in the upper layer (0–150 m), middle layer (150–250 m) and bottom layer (>250 m), respectively. Both the upper-layer and middle-layer circulations exhibit cyclonic anomalies during winter and anti-cyclonic anomalies from summer to autumn, and the circulation in the bottom layer flows cyclonically throughout the year with weak seasonality.

We linked effectively extrinsic and intrinsic forcings that control the layered circulation using novel LIVE dynamics. Vorticity imparts from wind stress curl in the upper layer, and a lateral planetary vorticity flux through the water exchanges at the straits surrounding the JS in all layers are the extrinsic forcings that dominate the structure and spatiotemporal variability of the layered circulation in the basin. The JEBAR effect arising from the slope flow interacting with topography serves as an important intrinsic dynamic response to the extrinsic flux. The torque generated by the pressure variation over variable bottom topography imparts vorticity into the water column, intrinsically affecting the strength of the circulation.

Similar layered-circulation structure has been found in low-latitude marginal seas, such as the South China Sea (Gan et al., 2016a) and the Banda Sea (Zhu et al., 2019). The main difference of the vorticity dynamics between the low-latitude and high-latitude marginal seas, is caused by β effect. The difference of planetary vorticity influx and outflux in the low-latitude marginal seas (e.g. the South China Sea and Banda Sea) is generally larger than that in the high-latitude waters (e.g. the JS). Thus, the contribution of the planetary vorticity net flux (Ω_{cor}) is relatively weak in the JS, as compared to the wind effect and other intrinsic dynamic processes.

Based on Stokes' circulation theorem, this study characterizes the layered circulation pattern and develops LIVE dynamics to effectively identify intrinsic and extrinsic forcing mechanism for the layered circulation for the JS and other marginal seas. In addition to the physical and dynamical aspects, layered circulation structure and its underlying mechanism discussed in this study also provide new understanding for biogeochemical substances transport. The horizontal influx of high nutrient concentration from TSM, and horizontal/vertical nutrient fluxes arising from the layered circulation are expected to affect the biological productivity in the euphotic layer and shape the nutrient distribution vertically, as shown in the SCS (Lu et al., 2020).

It should be noted that the horizontal resolution of ~8 km in CMOMS may not well resolve sub-mesoscale processes, which may affect the contribution of nonlinearity in the basin. Besides, a model with higher vertical resolution would better resolve the process in the bottom boundary layer. CMOMS with a higher resolution of ~3 km and vertically 60 σ-layers has been developing for future study.

CRediT authorship contribution statement

Junlu Li: Writing – review & editing, Writing – original draft, Visualization, Validation, Methodology, Investigation, Formal analysis, Data curation. **Jianping Gan:** Writing – review & editing, Supervision, Resources, Project administration, Methodology, Funding acquisition, Data curation, Conceptualization.

Declaration of competing interest

The authors declare that they have no known competing financial interests or personal relationships that could have appeared to influence the work reported in this paper.

Acknowledgements

This research was supported by the Center for Ocean Research in Hong Kong and Macau (CORE), a joint research center between Laoshan Laboratory and Hong Kong University of Science and Technology (Hong Kong, China). This work was also supported by grants from the Hong Kong Research Grants Council, including the Area of Excellence Scheme (AoE/P-601/23-N) and the General Research Fund (GRF 16310724). We are also grateful for the support of The National Supercomputing Center of Tianjin and Guangzhou. The CMOMS data used in the paper are produced by the Regional Ocean Modeling System (ROMS), and these data can be obtained from https://odmp.ust.hk/cmoms/.

Data availability

Data will be made available on request.

References

Byun, S.-K., Seung, Y., 1984. Description of current structure and coastal upwelling in the south-west Japan Sea-summer 1981 and spring 1982. In: Elsevier Oceanography Series. Elsevier, pp. 83–93.
Chang, K.-I., Hogg, N.G., Suk, M.-S., Byun, S.-K., Kim, Y.-G., Kim, K., 2002. Mean flow and variability in the southwestern East Sea. Deep Sea Res. Oceanogr. Res. Pap. 49, 2261–2279.
Carnes, M.R., 2009. Description and Evaluation of GDEM-V 3.0. Naval Research Laboratory, pp. 1–24. https://geo.gcoos.org/data/ts_profile/GDEMV-3.pdf.
Chang, K.-I., Teague, W.J., Lyu, S.J., Perkins, H.T., Lee, D.-K., Watts, D.R., Kim, Y.-B., Mitchell, D.A., Lee, C.M., Kim, K., 2004. Circulation and currents in the southwestern East/Japan Sea: overview and review. Prog. Oceanogr. 61, 105–156.
Fairall, C.W., Bradley, E.F., Hare, J., Grachev, A.A., Edson, J.B., 2003. Bulk parameterization of air–sea fluxes: updates and verification for the COARE algorithm. J. Clim. 16, 571–591.
Fukamachi, Y., Ohshima, K.I., Ebuchi, N., Bando, T., Ono, K., Sano, M., 2010. Volume transport in the Soya Strait during 2006–2008. J. Oceanogr. 66, 685–696.
Gamo, T., Horibe, Y., 1983. Abyssal circulation in the Japan Sea. J. Oceanogr. Soc. Jpn. 39, 220–230.
Gan, J., Allen, J.S., 2005. On open boundary conditions for a limited-area coastal model off Oregon. Part 1: response to idealized wind forcing. Ocean Model. 8, 115–133.
Gan, J., Liu, Z., Hui, C.R., 2016a. A three-layer alternating spinning circulation in the South China Sea. J. Phys. Oceanogr. 46, 2309–2315.
Gan, J., Liu, Z., Liang, L., 2016b. Numerical modeling of intrinsically and extrinsically forced seasonal circulation in the China Seas: a kinematic study. J. Geophys. Res.: Oceans 121, 4697–4715.
Han, S., Hirose, N., Usui, N., Miyazawa, Y., 2016. Multi-model ensemble estimation of volume transport through the straits of the East/Japan Sea. Ocean Dyn. 66, 59–76.
Isobe, A., Tawara, S., Kaneko, A., Kawano, M., 1994. Seasonal variability in the Tsushima warm current, Tsushima-Korea Strait. Cont. Shelf Res. 14, 23–35.
Ito, T., Togawa, O., Ohnishi, M., Isoda, Y., Nakayama, T., Shima, S., Kuroda, H., Iwahashi, M., Sato, C., 2003. Variation of velocity and volume transport of the Tsugaru Warm Current in the winter of 1999–2000. Geophys. Res. Lett. 30.
Kawabe, M., 1982. Branching of the tsushima current in the Japan Sea. J. Oceanogr. Soc. Jpn. 38, 95–107.
Kim, T., Yoon, J.-H., 2010. Seasonal variation of upper layer circulation in the northern part of the East/Japan Sea. Cont. Shelf Res. 30, 1283–1301.
Kim, Y.-G., Kim, K., 1999. Intermediate waters in the East/Japan Sea. J. Oceanogr. 55, 123–132.
Li, J., Gan, J., 2020. On the formation dynamics of the north equatorial undercurrent. J. Phys. Oceanogr. 50, 1399–1415.
Lie, H.J., Cho, C.H., 1994. On the origin of the Tsushima Warm Current. J. Geophys. Res.: Oceans 99, 25081–25091.
Liu, Z., Gan, J., 2016. Open boundary conditions for tidally and subtidally forced circulation in a limited-area coastal model using the Regional Ocean Modeling System (ROMS). J. Geophys. Res.: Oceans 121, 6184–6203.
Lu, Z., Gan, J., Dai, M., Zhao, X., Hui, C.R., 2020. Nutrient transport and dynamics in the South China Sea: a modeling study. Prog. Oceanogr. 183, 102308.

Matsuyama, M., Wadaka, M., Abe, T., Aota, M., Koike, Y., 2006. Current structure and volume transport of the Soya Warm Current in summer. J. Oceanogr. 62, 197–205.
Mellor, G.L., Yamada, T., 1982. Development of a turbulence closure model for geophysical fluid problems. Rev. Geophys. 20, 851–875.
Mertz, G., Wright, D.G., 1992. Interpretations of the JEBAR term. J. Phys. Oceanogr. 22, 301–305.
Miita, T., Ogawa, Y., 1984. Tsushima currents measured with current meters and drifters. In: Elsevier Oceanography Series. Elsevier, pp. 67–76.
Nishida, Y., Kanomata, I., Tanaka, I., Sato, S., Takahashi, S., Matsubara, H., 2003. Seasonal and interannual variations of the volume transport through the Tsugaru Strait. Umi no kenkyu 12, 487–499.
Sasaki, H., Nonaka, M., Masumoto, Y., Sasai, Y., Uehara, H., Sakuma, H., 2008. An eddy-resolving hindcast simulation of the quasiglobal ocean from 1950 to 2003 on the Earth Simulator. High Resolution Numerical Modelling of the Atmosphere and Ocean. Springer, pp. 157–185.
Senjyu, T., 1999. The Japan Sea intermediate water; its characteristics and circulation. J. Oceanogr. 55, 111–122.
Shchepetkin, A.F., McWilliams, J.C., 2005. The regional oceanic modeling system (ROMS): a split-explicit, free-surface, topography-following-coordinate oceanic model. Ocean Model. 9, 347–404.
Shin, C.W., Byun, S.K., Kim, C.S., 1996. Comparison between geostrophic currents and measured in the Southwestern part of the East Sea. J. Kor. Soc. Oceanogr. 31 (2), 89–96.
Takematsu, M., Nagano, Z., Ostrovski, A.G., Kim, K., Volkov, Y., 1999. Direct measurements of deep currents in the northern Japan Sea. J. Oceanogr. 55, 207–216.
Takikawa, T., Yoon, J.-H., Cho, K.-D., 2005. The Tsushima warm current through Tsushima Straits estimated from ferryboat ADCP data. J. Phys. Oceanogr. 35, 1154–1168.
Tawara, S., Miita, T., Fujiwara, T., 1984. The hydrography and variability in the Tsushima Straits. Bulletin on coastal oceanography 22, 50–58.
Teague, W.J., Jacobs, G., Perkins, H., Book, J., Chang, K., Suk, M., 2002. Low-frequency current observations in the Korea/Tsushima Strait. J. Phys. Oceanogr. 32, 1621–1641.
Teague, W.J., Tracey, K.L., Watts, D.R., Book, J.W., Chang, K.-I., Hogan, P.J., Mitchell, D. A., Suk, M.-S., Wimbush, M., 2005. Observed deep circulation in the Ulleung Basin. Deep Sea Res. Part II Top. Stud. Oceanogr. 52, 1802–1826.
Toba, Y., Omizawa, K.T., Kurasawa, Y., Hanawa, K., 1982. Seasonal and year-to-year variability of the Tsushima. La Mer 20, 41–51.
Yanagi, T., 2002. Water, salt, phosphorus and nitrogen budgets of the Japan Sea. J. Oceanogr. 58, 797–804.
Yi, S.-U., 1966. Seasonal and secular variations of the water volume transport across the Korea Strait. 한국해양학회지 1, 7–13.
Yoon, J.-H., Kawamura, H., 2002. The formation and circulation of the intermediate water in the Japan Sea. J. Oceanogr. 58, 197–211.
Yi, Z.H., 1982. Numerical experiment on the circulation in the Japan sea Part III. Mechanism of the nearshore branch of the Tsushima Current. J. Oceanogr. Soc. Jpn. 38, 125–130.
Zhu, Y., Wang, L., Wang, Y., Xu, T., Li, S., Cao, G., Qu, T., 2019. Stratified circulation in the Banda Sea and its causal mechanism. J. Geophys. Res.: Oceans 124, 7030–7045.